Investigation of Modal Iwan Models for Structures with Bolted Joints

Brandon J. Deaner, Matthew S. Allen
Graduate Research Assistant, Assistant Professor
Department of Engineering Physics
University of Wisconsin-Madison
535 Engineering Research Building
1500 Engineering Drive
Madison, WI 53706
bdeaner@wisc.edu, msallen@engr.wisc.edu

Michael J. Starr, Daniel J. Segalman
Sandia National Laboratories
Component Science and Mechanics
P.O. Box 5800
Albuquerque, NM 87185 and Livermore, CA 94550
mjstarr@sandia.gov, djsegal@sandia.gov

ABSTRACT

Structures with mechanical joints are difficult to accurately model; even when the natural frequencies of the system remain essentially constant, the damping introduced by the joints is often observed to depend nonlinearly on amplitude. Although models for individual joints have been employed with some success, the modeling of a structure with many joints remains a significant obstacle. This work explores whether nonlinear damping can be applied in a modal framework, where instead of modeling each discrete joint within a structure, a nonlinear damping model is used for each mode of interest. This approach assumes that the mode shapes of the structure do not change significantly with amplitude and that there is negligible coupling between modes. The nonlinear Iwan joint model has had success in modeling the nonlinear damping of individual joints and is used as a modal damping model in this work. The proposed methodology is first evaluated by simulating a structure with a small number of discrete Iwan joints (bolted joints) in a finite element code. A modal Iwan model is fit to simulated measurements from this structure and the accuracy of the modal model is assessed. The methodology is then applied to actual experimental hardware with a similar configuration and a modal damping model is identified for the first few modes of the system. The proposed approach seems to capture the response of the system quite well in both cases, especially at low force levels when macro-slip does not occur.

Keywords: nonlinear damping, bolted joints, Iwan model, energy dissipation, modal damping.

1. Introduction

Mechanical joints are known to be a major source of damping in jointed structures. However, the physics at the interface are quite complex and the amplitude dependence of damping in mechanical joints has proven quite difficult to predict. For many systems, linear damping models seem to capture the response of a structure at calibrated force levels. However, that approach relies on testing the structure at large force levels to calibrate the model. Furthermore, that approach can be over conservative or even erroneous since a linear model does not capture the amplitude dependence of the damping. Thus, it is crucial to understand how mechanical joints behave at a range of force levels so that the response of a jointed structure can be modeled accurately.

In this work, nonlinearities associated with mechanical joints will be classified into two different regions, micro-slip and macro-slip. Consider the joint shown in Fig. 1, where a bolt is used to connect two slabs of material. The preload in the bolt creates a contact region between the two slabs near the bolt. If a force F is applied to the slabs, slip will occur at the outskirts of the contact region. This means that there will be a region of stick and a region of slip as indicated in Fig. 1. For this case,

the bolted joint is said to be undergoing micro-slip due to the small slip displacements that cause the frictional energy loss [1].

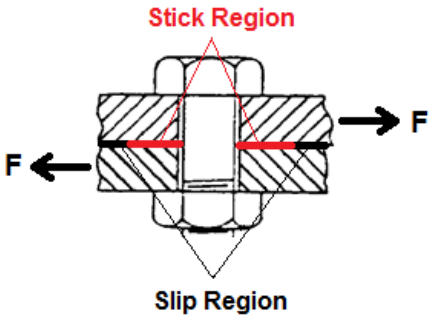

Fig. 1 Contact and Slip regions are shown for a mechanical joint undergoing micro-slip [1].

Macro-slip occurs when the stick region vanishes and larger slip displacements are possible. If a very large displacement is considered, the slabs of material will eventually come into contact with the bolt. This further complicates the system and is not considered in this work.

To capture the response of the joint in both the micro-slip and macro-slip regions, a 4-Parameter Iwan model was developed in [2]. This constitutive model has a small number of parameters and yet accounts for the key characteristics of the joint's response including the joint slip force (F_S), joint stiffness (K_T), and power law energy dissipation (χ, β). In the past decade, the 4-Parameter Iwan model has been implemented to predict the vibration of structures with a few discrete joints [3, 4]. However, when modeling individual joints, each joint requires a unique set of parameters $\{F_S, K_T, \chi, \beta\}$, which means that hundreds or even thousands of joint parameters may need to be deduced for the systems of interest. On the other hand, when a small number of modes are active in a response, some measurements have suggested that a simpler model may be adequate. Segalman investigated the idea of applying the 4-Parameter Iwan model in a modal framework in [5]. He used simulated measurements to deduce the modal Iwan parameters for two simple spring mass systems and compared this to the more rigorous approach where each discrete joint in the system was treated separately.

This work builds on Segalman's work [5] by simulating a more realistic finite element structure. First, a structure with four discrete Iwan joints is modeled using finite elements and the simulated response data is used to deduce a set of modal Iwan parameters. Particular attention is given to the degree to which the modal Iwan model captures the response of the finite element model that includes discrete Iwan joints. The methodology is then applied experimentally to an actual beam with a small link attached through two bolted joints. The beam was tested with free-free conditions, and great care had to be taken to assure that the suspension system did not dominate the measured damping. The initial results are promising, revealing that the modal Iwan approach does capture the response of the actual structure quite well in the micro-slip regime.

2. Nonlinear Energy Dissipation Model

The 4-Parameter Iwan model that is used in this work was initially presented in [2]. A historical review of the major contributors prior to Iwan's work led to the Iwan model being referred to as the Bauschinger-Prandtl-Ishlinskii-Iwan (BPII) model in a more recent work [6]. However, for simplicity and consistency with previous works, in this work the constitutive model will be referred to as the Iwan model.

2.1 Parallel-Series Iwan Model

A parallel arrangement of elements, each composed of a spring and frictional damper in series, is referred to as a parallel-series model in [7]. The physical representation of a parallel-series Iwan model is shown in [2]. The force in the joint, $F(t)$, is shown to have the following form,

$$F(t) = \int_0^\infty \rho(\phi)\left[u(t) - x(t,\phi)\right] d\phi \tag{1}$$

where

$$\dot{x}(t,\phi) = \begin{cases} \dot{u} & \text{if } \left\|u - x(t,\phi)\right\| = \phi \quad \text{and} \quad \dot{u}\left[u - x(t,\phi)\right] > 0 \\ 0 & \text{otherwise} \end{cases} \tag{2}$$

and $u(t)$ is the extension of the joint, $x(t,\phi)$ is the displacement of the frictional damper with strength ϕ and $\rho(\phi)$ is the population density of the spring and frictional damper elements with strength ϕ.

The response properties of the Iwan joint are characterized by the population density $\rho(\phi)$. Various population densities and their limitations are discussed in [6, 8]. Experiments at small force levels have revealed that the energy dissipated by the joint over one vibration cycle tends to be a power of the applied force. Analytically, the energy dissipation associated with pure material damping yields a power of 2.0, while the energy dissipation associated with friction between two bodies when the contact pressure is uniform yields a power of 3.0 [1, 2, 9, 10]. Experimentally, the dissipation tends to have a power-law slope that ranges between 2.0 and 3.0 [10]. One explanation for why experimental results often dissipate energy at a power less than 3.0 is due to the presumption that the contact pressure is nonuniformly distributed in joints [9].

In any event this means that at small force levels, a population density that dissipates energy in a power-law type fashion is desired. At large force levels, joints are known to exhibit a discontinuous nonlinearity associated with the initiation of macro-slip. This characteristic of joints must also be accounted for by the population density.

2.2 4-Parameter Iwan Model

To accommodate the behavior of joints at a large range of forces, a 4-parameter population density was developed in [2] with the form:

$$\rho(\phi) = R\phi^{\chi}\left[H(\phi) - H(\phi - \phi_{\max})\right] + S\delta(\phi - \phi_{\max}) \tag{3}$$

where $H(\ )$ is the Heaviside step function, $\delta(\ )$ is the Dirac delta function and the four parameters that characterize the joint include: R, which is associated with the level of energy dissipation, χ, which is directly related to the power law behavior of energy dissipation, $\phi_{\max}$, which is equal to the displacement at macro-slip, and the coefficient S, which accounts for a potential discontinuous slope of the force displacement plot when macro-slip occurs.

The four parameters $\{R, \chi, \phi_{\max}, S\}$ are converted to more physically meaningful variables $\{K_T, F_S, \chi, \beta\}$ in [2, 4]. F_S is the joint force necessary to initiate macro-slip, K_T is the stiffness of the joint, χ is directly related to the slope of the energy dissipation in the micro-slip regime, and β relates to the level of energy dissipation and the shape of the energy dissipation curve as the macro-slip force is approached.

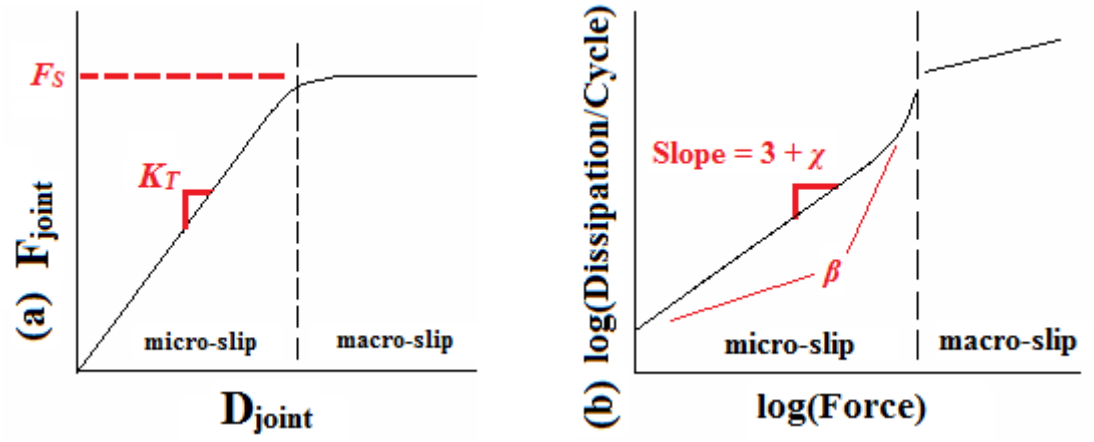

Fig. 2 (a) Both macro-slip force (F_S) and joint stiffness (K_T) can be found from the force-displacement relationship of the joint. (b) The χ value is found from the slope of the dissipation and the β value is a measure of dissipation level and shape of the dissipation curve.

This new set of parameters, $\{K_T, F_S, \chi, \beta\}$, can be deduced from the two plots seen in Fig. 2. Given a set of simulation or experimental data, there are a variety of methods that could be used to find the energy dissipation and joint force. A few of these methods will be highlighted in Section 2.4. Once these are known, the Iwan parameters can be determined graphically, or using nonlinear optimization as discussed in [2], or through some combination of the two. This work focuses on the graphical approach as it lends more insight into the importance of each parameter and its validity.

If we consider a system where the damping is strictly due to the 4-Parameter Iwan model, the governing equation becomes

$$M\ddot{x} + K_{\infty}x = F^{X} + F^{J} \tag{4}$$

where M and K_∞ are the linear mass and stiffness matrices of a finite element model, F^X is the vector of external forces, and F^J is a vector of nonlinear joint forces that the joint applies to the structure. Note that F^J is the 4-parameter Iwan model defined in Eq. (1) with opposite sign convention. F^J has nonzero entries corresponding to the two ends where the joint is attached to the finite element model and depends on the displacement at those points.

As discussed previously, the 4-parameter Iwan model has been implemented to predict the response of structures with a small number of discrete joints [3, 4]. However, each joint requires a unique set of parameters $\{K_T, F_S, \chi, \beta\}$, so many joint parameters need to be deduced and it is not likely that they can all be determined uniquely from a set of experimental measurements.

2.3 Modal Iwan Model

In order to circumvent this limitation, Segalman proposed that energy dissipation be applied on a mode-by-mode basis, using the 4-parameter Iwan constitutive model [5]. The Iwan model is assumed to be applicable to each mode, although the parameters of each mode are tuned to match experimental measurements and hence aren't necessarily the same as the parameters of any individual joint in the structure. In general, the nonlinearity that joints introduce can couple the modes of a system so that modes in the traditional linear sense can not be defined. However, experiments have often shown that structures with joints are typically quite linear, suggesting that one might be able to model the structure as a collection of uncoupled linear modes, each with nonlinear damping characteristics. This would allow one to model a structure with a relatively small number of modes that capture its performance in the frequency band of interest, and the response of each mode could be found through a nonlinear, single degree-of-freedom simulation. Specifically, each modal degree-of-freedom is modeled by a single degree-of-freedom oscillator, as shown in Fig. 3, with a 4-parameter Iwan model placed between the modal degree of freedom and the ground. A second spring is placed in parallel with the 4-parameter Iwan model, representing the residual stiffness of that mode when the Iwan model is in macro-slip.

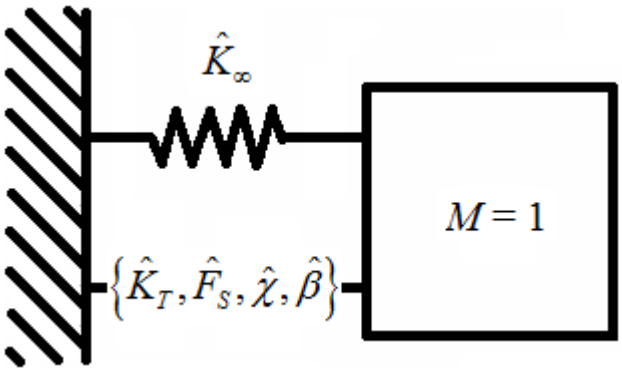

Fig. 3 Schematic of the model for each modal degree of freedom. Each mode has a unique set of Iwan parameters that characterize its nonlinear damping (and to a lesser extent stiffness).

Again, the modal Iwan parameters $\{\hat{K}_T, \hat{F}_S, \hat{\chi}, \hat{\beta}\}$ in Fig. 3 will not be the same as the $\{K_T, F_S, \chi, \beta\}$ parameters of any discrete Iwan joint parameters in the structure.

The response for each mode r is then governed by the following differential equation,

$$\ddot{q}_r + \omega_{0,r}^2 q_r = \Phi_r{}^{\mathrm{T}} F^X + \hat{F}_{J,r} + \hat{K}_{T,r} q_r \tag{5}$$

where Φ_r and ω_0 are found by solving the eigenvalue problem $\left[[K_0] - \omega_{0,r}^2\right]\Phi_r = 0$ and $\hat{F}_{J,r}$ is the modal joint force and $\hat{K}_{T,r}$ is the modal joint stiffness for the r^{th} mode. The low force mode shapes are used to define the modal parameters, so the stiffness matrix used in the eigenvalue problem above must include the low-force stiffness of the joints, i.e. $[K_0] = [K_\infty] + [K_T]$, where $[K_T]$ is a matrix that captures the stiffness that the joints contribute to the structure when the load is infinitesimal. This presumes that the stiffness of the joints has been included when calculating the mode shapes Φ_r and natural frequencies ω_0 of the structure (i.e. the modal Iwan model exhibits no slip). In practice, these modal parameters will come from a low-level modal test and so this assumption should be valid. On the other hand, if the structure is modeled

in finite elements then the stiffness of the joints should be included when calculating the mode shapes; this functionality is built into the Sierra/SD (Salinas) finite element package [11, 12].

2.4 Extracting Frequency and Energy Dissipation Data

In this work, the modal Iwan parameters $\left\{\hat{K}_T, \hat{F}_S, \hat{\chi}, \hat{\beta}\right\}$ will be extracted by estimating the frequency and energy dissipation from the free response of each mode of interest. Two methods for calculating frequency and energy dissipation were explored in this work.

2.4.1 Peak-Picking and Zero-Crossing Approach

The first method was developed by Segalman in an unpublished document. The time history of the acceleration is approximated as

$$a(t) = e^{P(t)} \cos\left(\omega(t)t\right) \tag{6}$$

where $e^{P(t)}$ is the envelope of the response, and $\omega(t)$ is the instantaneous frequency. The envelope $e^{P(t)}$ is found by identifying the acceleration peaks and fitting a cubic spline to the logarithm of those peaks. The frequency $\omega(t)$ is found by calculating the zero-crossings of a response. The energy dissipation per cycle is calculated using the change in peak kinetic energy and is given by

$$KE_P = \frac{M}{2} v_P^2 = \frac{M}{2} \frac{e^{2P(t)}}{\omega^2} \tag{7}$$

where v_P is the peak velocity of each cycle. The change in peak kinetic energy is calculated by taking the derivative of the peak kinetic energy which is then multiplied by the period ($2\pi/\omega$) to estimate the energy dissipation per cycle D. This assumes that kinetic energy changes slowly relative to the period so that it can be approximated as constant over each cycle.

$$D \approx \frac{dKE_P}{dt} \frac{2\pi}{\omega} = \frac{4\pi}{\omega} \frac{dP(t)}{dt} KE_P \tag{8}$$

2.4.2 Hilbert Transform with Polynomial Smoothing Approach

The second method uses the Hilbert transform along with curve fitting to smooth the instantaneous phase and amplitude found from a Hilbert transform [13, 14]. An analytic signal is formed when the Hilbert transform, $\tilde{a}(t)$, is added to the acceleration response [15]

$$A(t) = a(t) + i\tilde{a}(t) \tag{9}$$

The magnitude of the analytic signal is the envelope of the response and is approximated by

$$Z(t) = \left|A(t)\right| = A_0 \exp\left(-\zeta(t)\omega_n(t)\right) \tag{10}$$

where A_0 is the initial amplitude, $\omega_n(t)$ is the frequency, and $\zeta(t)$ is the coefficient of critical damping. The instantaneous phase is obtained from the analytic signal using the following equation.

$$\varphi(t) = \tan^{-1}\left(\frac{\tilde{a}(t)}{a(t)}\right) \tag{11}$$

In other works, for example those by Feldman [15], the instantaneous natural frequency is apparently found by low-pass filtering and then differentiating the phase. However, those works give little detail regarding the optimal low-pass filter and the results depend heavily on the filter used. If the response is not filtered then noise in the measured response is amplified by the differentiation making the results meaningless, even when the noise is quite small (e.g. integration error in the simulations presented here). In this work, the measured phase is smoothed by fitting a polynomial to the data before differentiating [13]. In addition, the beginning and end of the phase data are deleted since they tend to be contaminated by end effects in the Hilbert Transform.

Both methods for extracting the frequency and energy dissipation data were explored in this work. In general, the Hilbert Transform with Curve Fitting approach was found to smooth out the data more effectively than the peak-picking/zero-crossing approach and will be used in the plots shown in this paper.

2.5 Deducing Modal Iwan Parameters

This section explains how modal Iwan parameters are deduced from energy dissipation versus force measurements. The procedure closely follows that used by Segalman in [5] and the work done by Guthrie, which was described in an unpublished memo. The methods described in the previous section provide a set of frequency and energy dissipation data such as that shown schematically in Fig. 4. Note that these are quite similar to those shown in Fig. 2 for a discrete joint, except that all of the quantities, such as the slip force, are now in a modal form rather than physical.. Also, since the modal Iwan model has a linear spring in parallel, its stiffness does not go to zero at macro-slip but instead it simply drops to K_∞.

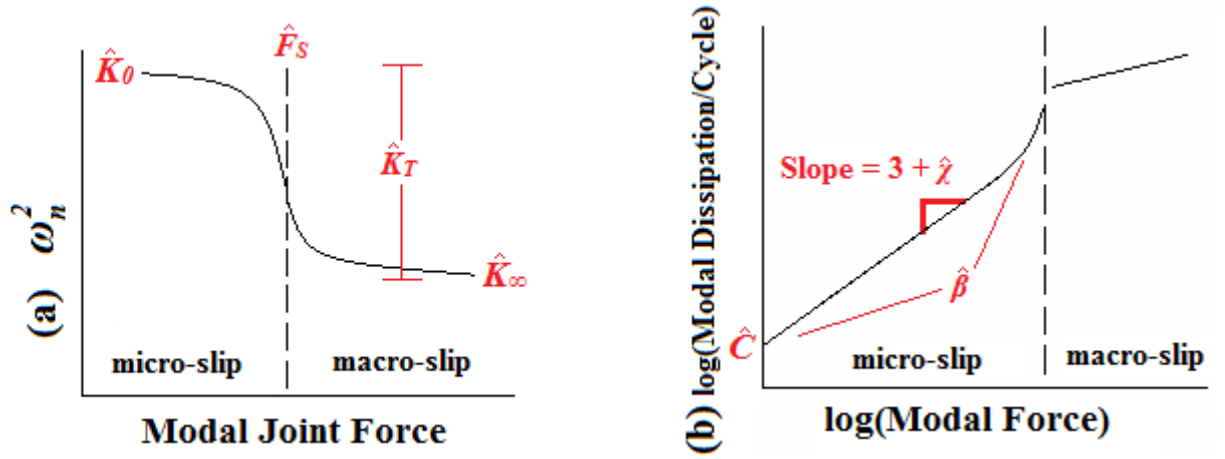

Fig. 4 (a) Modal macro-slip force ($\hat{F}_S$) and modal joint stiffness ($\hat{K}_T$) can be found from the softening seen in the natural frequency. (b) The $\hat{\chi}$ value is found from the slope of the modal dissipation and the $\hat{\beta}$ value is a measure of modal dissipation level and shape of the modal dissipation curve.

The $\hat{\chi}$ parameter is found by fitting a line to the data for the log of energy dissipation versus log of the modal force at low force levels. Then the $\hat{\chi}$ parameter for each mode *r* is given by the slope of that line minus three:

$$\hat{\chi}_r = \text{Slope}_r - 3 \tag{12}$$

In order to deduce the Iwan modal stiffness $\hat{K}_T$, the natural frequencies of each mode are plotted versus modal joint force. A softening of the system, characterized by a drop in frequency, illustrates the amount of modal stiffness associated with all the relevant joints of the system. Assuming that the mode shapes used in the modal filtering process are mass normalized, the equation for modal joint stiffness for each mode becomes

$$\hat{K}_{T,r} = \hat{K}_{0,r} - \hat{K}_{\infty,r} = \omega_{0,r}^2 - \omega_{\infty,r}^2 \tag{13}$$

where ω_0 is the natural frequency corresponding to the case when all the joints in the structure exhibit no slipping, and ω_∞ is the natural frequency when all of the joints are slipping. This points to the major advantage of using a modal Iwan implementation as opposed to a discrete Iwan implementation. For a modal Iwan implementation, only the modal stiffness and modal slip force of each kept mode needs to be considered as opposed to calculating the stiffness and slip force associated with each joint individually.

The modal joint slip force, $\hat{F}_S$, can be estimated from Fig. 4a. To find the last parameter, $\hat{\beta}$, all of the previous parameters found are needed along with the y-intercept, $\hat{C}$, of the line that was fit in order to find the $\hat{\chi}$ parameter. Then, the following equation was formed from [2] that can be used to solve for $\hat{\beta}$ numerically.

$$\hat{F}_{s,r} = \left[\frac{4\left(\hat{\chi}_r + 1\right)\hat{K}_{T,r}^{\chi_r+2}\left(\hat{\beta}_r + \dfrac{\hat{\chi}_r + 1}{\hat{\chi}_r + 2}\right)^{\hat{\chi}_r+1}}{\hat{C}_r K_{\infty,r}^{(3+\hat{\chi}_r)}\left(2+\hat{\chi}_r\right)\left(3+\hat{\chi}_r\right)\left(1+\hat{\beta}_r\right)^{\hat{\chi}_r+2}} \right]^{\frac{1}{\hat{\chi}_r+1}} \tag{14}$$

Once all of these parameters have been determined, one can reconstruct the modal energy dissipation versus force curve for the modal Iwan model and compare it to the measurements. This is helpful, since experience has revealed that it is sometimes necessary to adjust the parameters $\{\hat{K}_T, \hat{F}_S, \hat{\beta}\}$ so that the dissipation versus force curve accurately fits the measurements. In the micro-slip region, the modal energy dissipation per cycle, $\hat{D}_r$, is adapted from [2] and is given by,

$$\hat{D}_r = 4\hat{r}_r^{\hat{\chi}_r+3}\left(\frac{\hat{F}_{S,r}}{\hat{K}_{T,r}}\right)\left(\frac{(\hat{\beta}_r+1)(\hat{\chi}_r+1)}{\left(\hat{\beta}_r + \dfrac{\hat{\chi}_r+1}{\hat{\chi}_r+2}\right)^2\left(\hat{\chi}_r+2\right)\left(\hat{\chi}_r+3\right)}\right) \tag{15}$$

where $\hat{r}_r$ is found by iteratively solving:

$$\frac{\hat{F}_{J,r}}{\hat{F}_{S,r}} = \hat{r}_r\left(\frac{(\hat{\beta}_r+1) - \dfrac{\hat{r}_r^{\hat{\chi}_r+1}}{\hat{\chi}_r+2}}{\hat{\beta}_r + \dfrac{\hat{\chi}_r+1}{\hat{\chi}_r+2}}\right) \tag{16}$$

For the macro-slip region, modal energy dissipation is given by:

$$\hat{D}_r = 4q_{p,r}\hat{F}_{S,r} \tag{17}$$

where $q_{p,r}$ is the peak modal displacement over a cycle of the response.

3. Finite Element Simulations

Both the discrete 4-parameter Iwan model and the modal Iwan model have been implemented into Sierra/SD (Salinas), a structural dynamics finite element code developed by Sandia National Laboratories [11, 12]. Sierra/SD was used to simulate the response of a structure with several discrete Iwan joints, in order to generate response data that was then fit to a modal Iwan model. Then the response of the modal Iwan model could be compared to that of the truth model to evaluate the proposed procedure.

3.1 Finite Element Model

The model of interest is a beam with a link attached to the center of the beam. The general dimensions of the beam (20" x 2" x 0.25") and link (3.5" x 0.5" x 0.125") are shown in Fig. 5. The beam is meshed with fairly course hexahedron elements (approximate edge length varies between 0.125" and 0.25") with a total of 1,554 nodes to keep the computational cost reasonable. The first five natural frequencies of this model were compared to the natural frequencies of a finely meshed model containing 37,553 nodes, and it was found that the error was less than 1%.

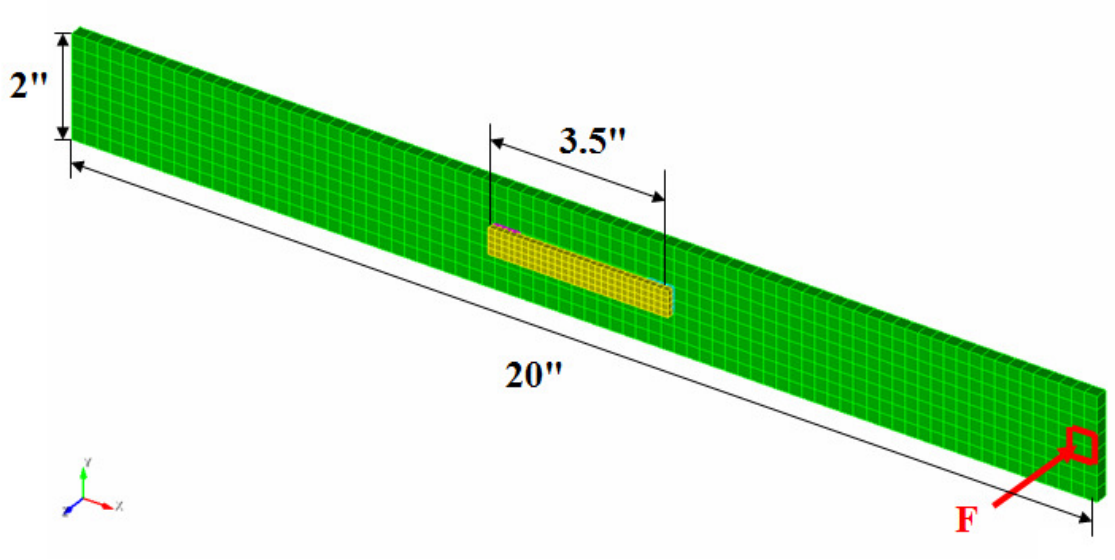

Figure 5: Computational model of a beam with several discrete Iwan joints.

The representative model has four square washers in contact with the beam as seen in Fig. 6. Four Iwan elements are defined for the two in-plane shear directions at the contact patches between the washers and the beam. Note that no other damping is included in this model, so for the discrete Iwan simulations, all of the energy dissipation is due to the Iwan model.

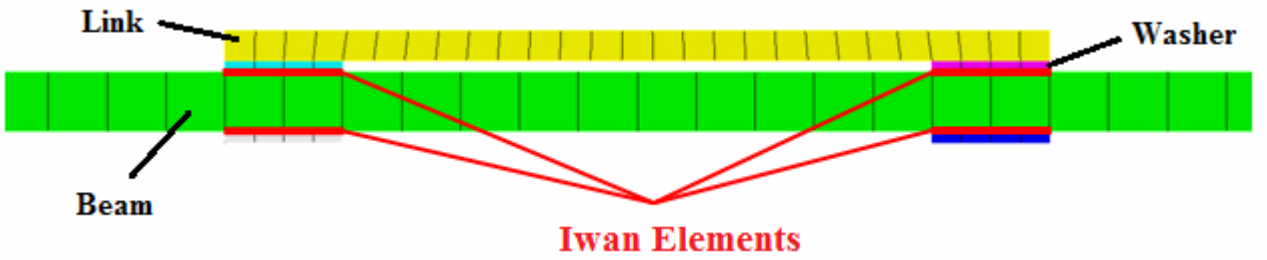

Fig. 6 Location of discrete Iwan joints. An Iwan joint is used at each surface where the washers come into contact with the beam.

In addition to the Iwan elements defined in the in-plane directions, constraints are placed on all out-of-plane rotations and displacements to prevent penetration and separation between the washers and the beam. Two of the washers are merged to the link which adds stiffness to the beam. The beam, link, and washers are given the linear elastic material properties of Stainless Steel 304.

3.2 Discrete Iwan Simulations

An experiment was simulated by exciting the finite element model with an impulsive force. The force was applied to nine nodes at the tip of the beam as shown in Fig. 5. A haversine forcing function was used with a duration of 1.6 ms. The duration of the force was chosen to primarily excite the first three elastic modes of vibration which will be analyzed in this work.

The acceleration time histories at all nodes were extracted and filtered using the pseudo inverse of the mode shape matrix including the first 50 mode shapes from a linear eigenanalysis. This was accomplished using a modal filter [16], i.e. by approximating the response as follows,

$$\ddot{x} = \Phi \ddot{q} \tag{18}$$

where Φ is the mode shape matrix including the first 50 linear modes, and then pre-multiplying both sides of Eq. (18) with the pseudo-inverse of the mode shape matrix.

The discrete Iwan parameters used for these simulations were those found from previous experimental studies of a lap joint [2]. The parameters for all four discrete Iwan elements are shown in Table 1.

Table 1: Iwan parameters used for the discrete Iwan simulations.

K_T (lb/in)	F_S (lb)	χ	β
$2.75 \cdot 10^5$	300	-0.3	0.02

3.3 Modal Iwan Simulations

The methodology described in Sec. 2.5 was then used to deduce the modal Iwan parameters of the first three elastic bending modes. The modal Iwan model was then used to predict the response of the system to the impulsive force used for the discrete Iwan simulations. This was done using the implementation of the modal Iwan model in the Sierra/SD finite element code. Hence, it was fairly straightforward to obtain the response of the modal model at every node of the finite element model. The modal coordinate amplitudes were not provided directly, so they were estimated from the acceleration time histories using the same process described previously. Both simulations were integrated using a Newmark-Beta integration scheme with an iterative Newton loop to solve the residual force equation. The step size was set to $1 \cdot 10^{-5}$ seconds with 20,000 time steps for a total time history of 0.2 seconds.

3.4 Simulation Results

The response of the truth model (i.e. that in Sec. 3.2) was modally filtered and the modal energy dissipation versus force was found using the procedure described in Sec. 2.4. The modal joint stiffness $\hat{K}_T$ and modal macro-slip force $\hat{F}_S$ were then estimated from this data, shown in Fig. 7. Fig. 7a shows the frequency versus modal joint force, $\hat{F}_J$ in Eq. (5), was estimated from the simulated measurements. Fig. 7b shows the modal energy dissipation, $\hat{D}$ in Eq. (8), versus modal joint force. Notice that the joint transitions to macro-slip over a range of forces so the modal slip force cannot be determined precisely. The modal Iwan parameters were deduced using the procedure described in Sec. 2.5, and the parameters obtained are shown in Table 2 for the first three elastic bending modes.

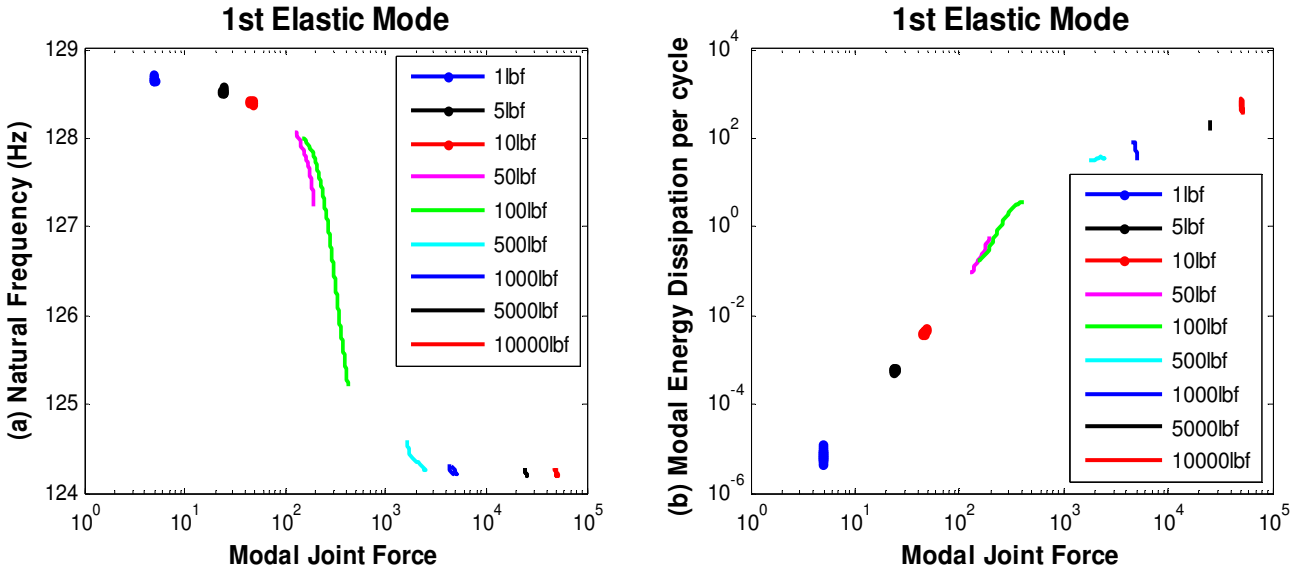

Fig. 7 Natural frequency (a) and energy dissipation (b) versus modal joint force for the 1st elastic mode of the finite element model. The change in the natural frequency observed in (a) is used to find the modal joint stiffness ($\hat{K}_T$) and the sharp change in slope in (b) is used to find the modal macro-slip force ($\hat{F}_S$).

Table 2: Iwan parameters used for the discrete Iwan simulations.

Mode	$\hat{K}_T$	$\hat{F}_S$	$\hat{\chi}$	$\hat{\beta}$
1st Elastic	$4.45 \cdot 10^4$	239.4	-0.183	0.3
2nd Elastic	$2.0 \cdot 10^4$	$1.0 \cdot 10^5$	-0.999	3.0
3rd Elastic	$8.73 \cdot 10^5$	534.6	-0.048	0.38

3.4.1 Comparison of Modal Time Responses

Now that the modal model has been identified, one can compare its response to that of the finite element truth model in Sec. 3.2. To simplify the comparison, the modal responses of the first mode were first assessed with impact force levels of 10lbf and 1000lbf, and the comparison is shown in Fig. 8. The modal responses agree very precisely at the 10lbf level. On the other hand, when an impact force with an amplitude of 1000lbf is applied to the model, the modal Iwan model seems to damp the response more than the discrete Iwan model. It is also interesting to note the sharp initial increase in modal acceleration due to the impact force, which seems to be well captured at both force levels.

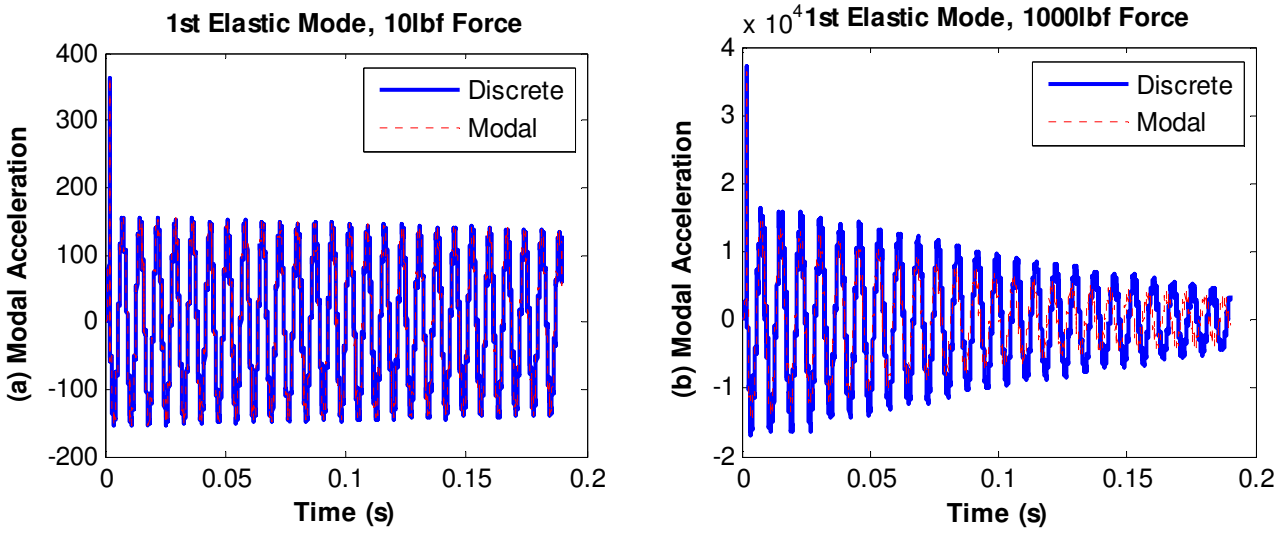

Fig. 8 Comparison of the response of the first elastic mode for both the Modal and Discrete Iwan models for impact forces of 10lbf (a) and 1000lbf (b).

It becomes clear that one would have to compare a large number of time histories to assess the performance of the modal Iwan model over the force range of interest. It is more effective to compare the modal energy dissipation that each model gives over the entire range of modal force. The energy dissipation of the modal Iwan model was computed using Eq. (15) through (17) and compared to that used to construct the model, as shown in Fig. 9.

3.4.2 Comparison of Modal Energy Dissipation

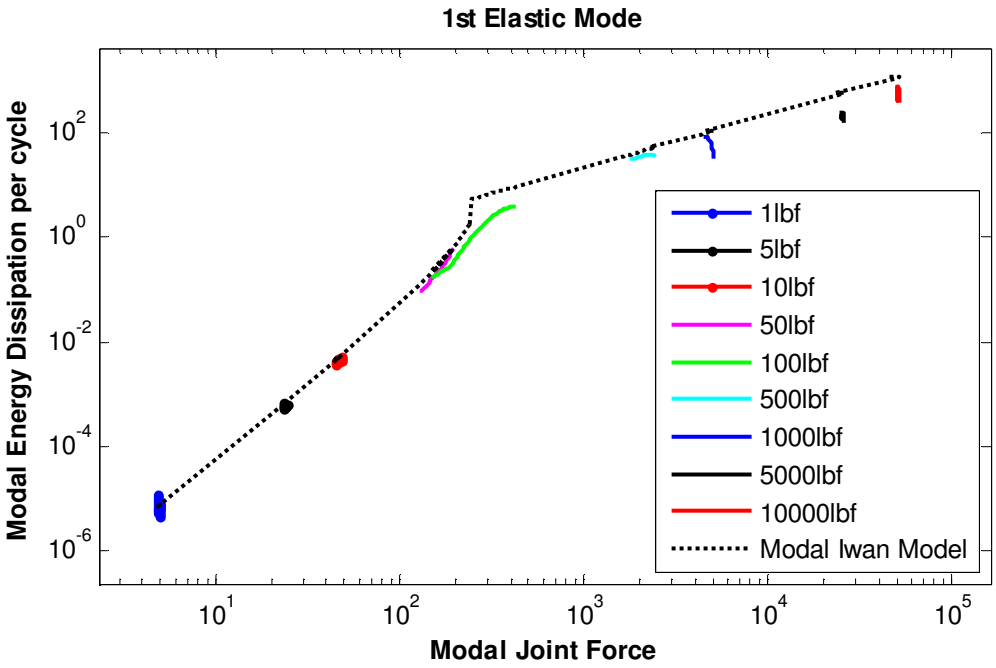

Fig. 9 Modal energy dissipation versus modal force for the 1st elastic mode. The colored lines show simulations of the finite element truth model (with discrete Iwan joints) and the black dashed line shows the dissipation for the modal Iwan model. The two compare well for a range of impact forces from 1lbf to 10,000lbf.

The comparison for the 1st elastic mode, in Fig. 9, reveals that the modal Iwan model does a very good job of predicting the energy dissipation for a range of impact loads that span the micro-slip and macro-slip regions. However, the data at higher force levels shows considerable scatter and the agreement is not as good at those force levels. This is why the comparison in Fig. 8 showed the modal Iwan model over-predicting the damping in the system at high force levels. Based on Fig. 9, one would expect a similar level of disagreement at 5,000 and 10,000lbf.

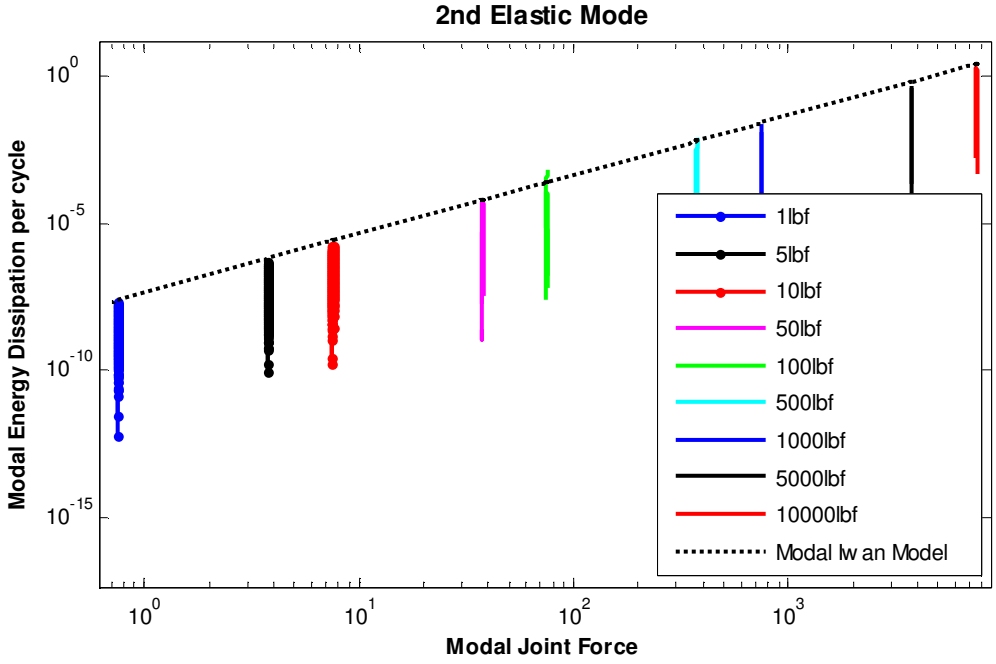

Fig. 10 Modal energy dissipation versus modal force for the 2nd elastic mode. The 2nd bending mode is lightly damped and the fit reveals that this mode can be well approximated as linear.

The modal energy dissipation versus force for the second elastic mode is shown in Fig. 10. There are several interesting features in this plot. First notice how each simulation's energy dissipation seems to drop to essentially zero towards the end of each time record. Each time history was limited to 0.2 seconds due the small time step required and the large volume of data that was generated when each nodal time history was written to a file. Since there is an extremely small amount of damping in the 2nd bending mode, the fitted envelope has very little decay. Hence, the estimate of the energy dissipation is very sensitive to envelope fit by the Hilbert Transform algorithm. The slope of the modal Iwan model in Fig. 10 has a value of approximately 2 corresponding to a $\hat{\chi}$ value of -1 which is characteristic of a linearly damped system. Thus, the dissipation in this mode could be modeled with a linear mode and a linear modal damping ratio instead of a modal Iwan model. Apparently, the location of the link is such that the discrete Iwan joints are not exercised by this mode.

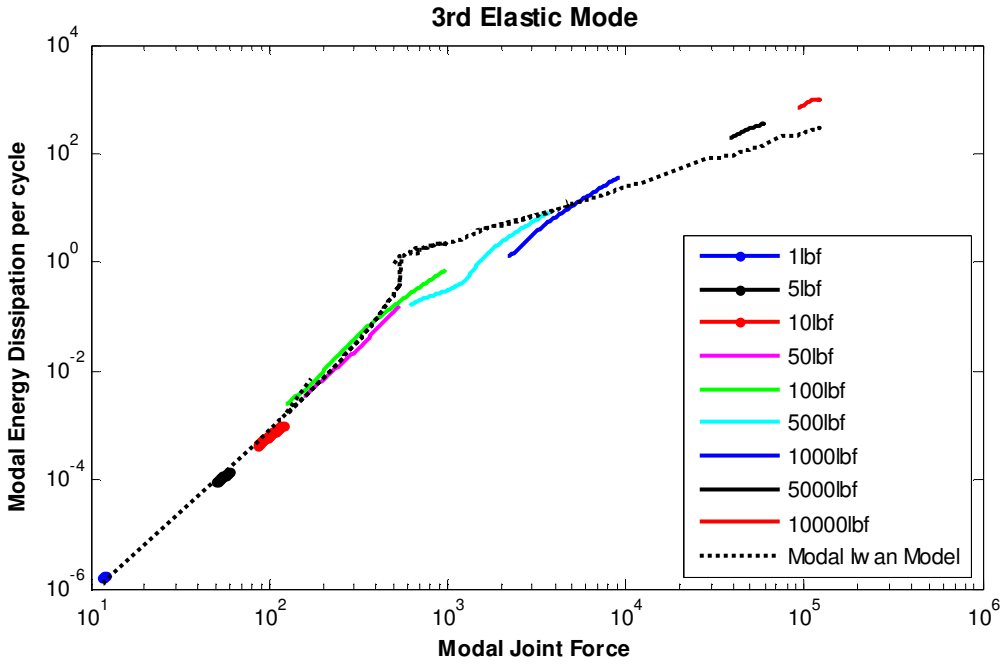

Fig. 11 Modal energy dissipation versus modal force for the 3rd elastic mode. The modal model agrees well with the discrete simulations for this mode in the micro-slip region, but not in the macro-slip region.

The comparison in Fig. 11 shows that the deduced modal Iwan model for the 3rd elastic mode does a very good job of predicting the energy dissipation in the micro-slip region, for which a $\hat{\chi}$ value of $\hat{\chi}_3$ = -0.048 was obtained. This value indicates quite a strong dependence on force (recall that each discrete joint had χ = -0.3. On the other hand, the modal Iwan model does a poor job of capturing the macro-slip region. The slope of the discrete Iwan simulations seems to be greater than the slope of the modal Iwan model in macro-slip. This suggests that Eq. (17) may not entirely describe the energy dissipation in the macro-slip region for this system. A similar effect was observed for some of the modes of the system studied in [5], the cause of which will be explored further in the future.

3.4.3 Discussion

These results validate the use of a modal Iwan model to capture the effect of discrete Iwan joints in the micro-slip region. On the other hand, the results suggest that the modal Iwan model may need to be modified to capture the response of a system at higher force levels corresponding to the macro-slip region. This is to be expected, perhaps, since the mode shapes used for the macro-slip region include joint stiffness; however, when the joints are in the macro-slip region the mode shapes should no longer include the joint stiffness. Also, the assumption of negligible modal interactions could very well be violated when the joints slip significantly.

4. Beam Experiments

The modal Iwan methodology was also assessed experimentally using experimental measurements from a free-free beam with a bolted link attached. The experimental setup was designed to minimize the effect of damping associated with the boundary conditions. Free boundary conditions were used because any other choice, e.g. clamped, would add significant

damping to the system. In Sec. 4.5, the energy dissipation characteristics of the modal Iwan model are compared with those of the actual experiment.

4.1 Test Structure

The structure tested in this work was first used by Sumali in [17]. The beam was designed to have the following characteristics: the structure had numerous modes from 0-2000 Hz, the modes are well separated in frequency and the modes do not switch order when the links are attached. Previously, a washer was inserted between the link and the beam as was done for the finite element model in Fig. 6. Initial tests were done in this configuration but the damping in the joint seemed linear, indicating that there was no slip present in the joint for the force levels tested. The washers were then removed in order to spread out the clamping force between the beam and the connecting element. The resulting configuration is shown in Fig. 12. This change seemed to cause the joint to slip more easily, so a greater degree of nonlinearity was observed. Also, the bolt torque for the original experiments was set between 80 and 110 inch-pounds which results in bolt preload force of approximately 1600-2200lbf. The bolt was tightened to a much lower torque of only 5 inch-pounds in these experiments.

The dimensions of the beam and link are the same as in the finite element model described in Sec. 3.1. However, there is no washer that separates the beam (20" x 2" x 0.25") from the link (3.5" x 0.5" x 0.125") as shown in Fig. 12. The bolts used to attach the link to the beam were 1/4"-28 fine-threaded bolts. All components were made of AISI 304 stainless steel.

Fig. 12 Schematic of the link and beam connection that was used in the experimental setup.

4.2 Lab Setup Challenges

The damping ratios of a freely supported structure are sensitive to the support conditions, as was explored in detail in [18]. Therefore, special attention must be given to the support conditions to assure that the damping that they add does not contaminate the results.

Initially, the beam was suspended by two strings that act as pendulum supports as was done in [18]. To prevent the rigid body modes from contaminating the elastic mode data, the pendulum motion of the beam should have a low natural frequency compared to the first elastic mode. The general rule of thumb states that the error in the measured natural frequencies will be less than 0.5% when the rigid body natural frequencies are less than one tenth of the elastic natural frequencies of interest. However, that same design theoretically produces 10% error in the measured damping ratios. A frequency ratio of approximately 20 was obtained when the beam was supported by only these two strings. Although this test provided a good baseline that was used to evaluate the damping of the boundary conditions in subsequent tests, there were practical considerations that prohibited its use for most of the testing.

Specifically, the velocity of the beam was measured with a scanning laser Doppler vibrometer in order to eliminate any damping associated with the cables of contact sensors. Hence, if the beam swings significantly in its pendulum mode, the point which the laser is measuring may change significantly during the measurement. Also, an automated hammer was used to excite the beam, but the hammer only retracts about one inch after impact. As a result, the pendulum motion of the beam caused almost unavoidable double hits with this setup. Finally, in the processing described subsequently, it is important for the automatic hammer to apply a highly consistent impact force. Any swinging of the beam caused the impact forces to vary from test to test and it was extremely difficult and time consuming to try to manually eliminate the swinging. For these reasons, soft bungee cords were used to suppress the rigid body motion of the beam while attempting to add as little damping as possible to the system. The final set up was similar to that used in [17] and is shown in Fig. 13. This setup was used for all of the measurements shown in this paper.

4.3 Experimental Setup

The dynamic response of the beam was measured using a Polytec Scanning Laser Doppler Vibrometer (PSV-400) to measure the response at 54 points on the beam. A Polytec single point Laser Doppler Vibrometer (OFV-534) was used to measure a reference point to verify that the hammer hits were consistent. The reference laser was positioned close to the impact force

location. An Alta Solutions Automated Impact Hammer with a nylon hammer tip was used to supply the impact force, which is measured by a force gauge attached between the hammer and the hammer tip.

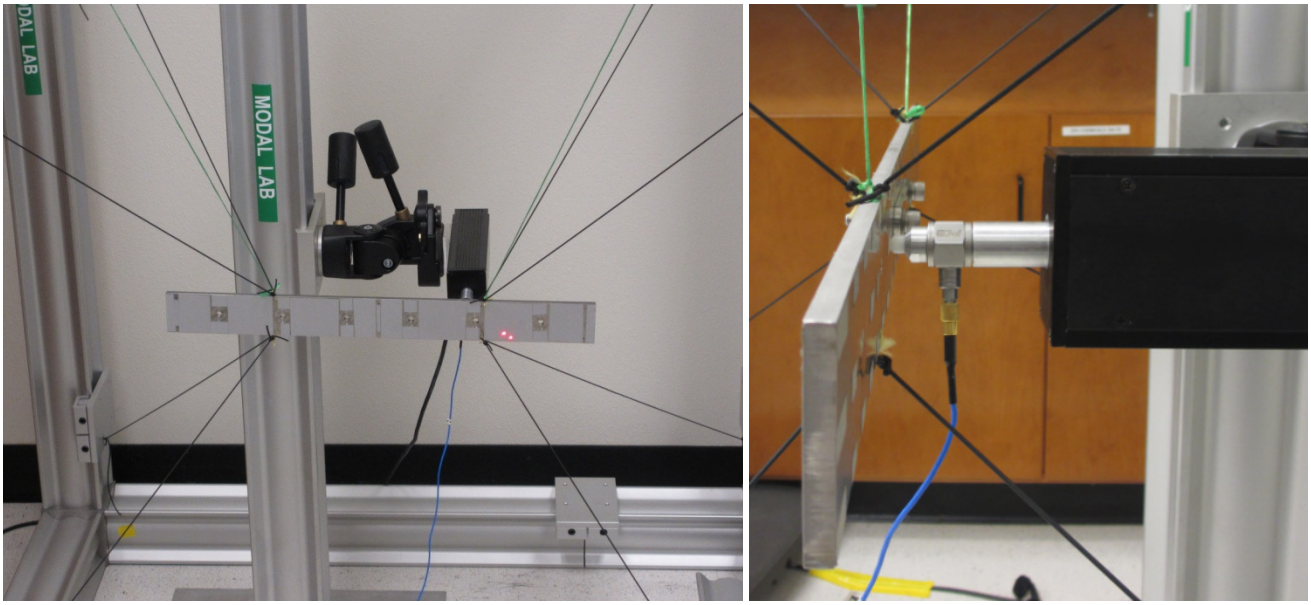

(a) (b)

Fig. 13 Photograph showing how the beam was suspended (a). Automatic hammer positioned behind the impact point. One link is attached to the beam and can be seen behind the hammer (b).

The beam is suspended by 2 strings that support the weight of the beam and the 8 bungee cords prevent excessive rigid-body motion. The bungees and strings were connected to the beam at locations where the odd bending modes have little motion in order to minimize damping in those modes. However, even after all of the care that was taken, some damping was added by the supports. A preliminary analysis was done in which the damping ratios of the first few modes of the beam were measured with and without bungees, and the results are shown in Table 3.

Table 3: Damping Ratios for the beam with and without bungees and with and without the link attached.

Mode	ζ without bungees and without link (%)	ζ without bungees with link at 50 in-lbf of torque (%)	ζ with bungees without link (%)	ζ with bungees with link at 5 in-lbf of torque (%)
1st Elastic	0.01	0.025	0.016	0.15
2nd Elastic	0.025	0.03	0.055	0.06
3rd Elastic	0.02	0.025	0.045	0.18

The damping of all of the modes is light, as one would expect for a monolithic structure with only a few bolted joints; the largest measured damping ratio was ζ=0.0006 for the second mode with the link and bungees attached. For the setup without bungees, the damping ratios of the first three elastic modes were found to increase slightly when the link was attached and the bolts were tightened to 50 in-lbf of torque. As discussed, a high torque will cause a large preload in the bolts which inhibits micro-slip. When the bungees were added to the setup, the damping ratios for all modes increased by a factor of between 1.6 and 2.3. For the first mode this is comparable to the increase in damping that was observed when the link was attached at 50 in-lb of torque, and it is considerably larger than the damping caused by the joint for modes 2 and 3. For this reason, the bolt torque was reduced to 5 in-lbf, causing the damping in the first mode to increase by an order of magnitude. The damping in the 2nd and 3rd modes increased to above what was observed for the beam without a link but with the bungees attached.

4.4 Lab Data Processing

A couple of approaches were explored to extract modal acceleration ring-downs from the laboratory data. Mass normalized mode shapes were found by fitting a linear modal model with the Algorithm of Mode Isolation (AMI) [19]. Then the mode shapes were used in a modal filter as in Eq. (18), as was done in Sec. 3.4. However, the modal responses obtained still showed clear evidence of frequency content due to other modes. Another approach that was explored was to band pass filter the data in the frequency domain in order to isolate a mode as was done in [14]. Although this approach seemed to work,

each measurement point had to be filtered and analyzed separately, and no averaging could be performed for all the measurement points since each point has a different magnitude associated with its mode shape value. In the end the measurements were band pass filtered in order to isolate each mode, as was done in [14], and then scaled by the corresponding mode shape value. A Butterworth filter was used in the band pass filtering process. The cut-off frequencies used for the first elastic mode were 120 and 135 Hz, and the FFT of the resulting filtered responses is shown in Fig. 14. The measurements at each point were then scaled by the corresponding mass normalized mode shape value in order to obtain a single average modal acceleration for each mode from the set of 54 measurement points. The resulting time responses are show in Fig. 15, as well as the average time response that was used to identify a modal Iwan model.

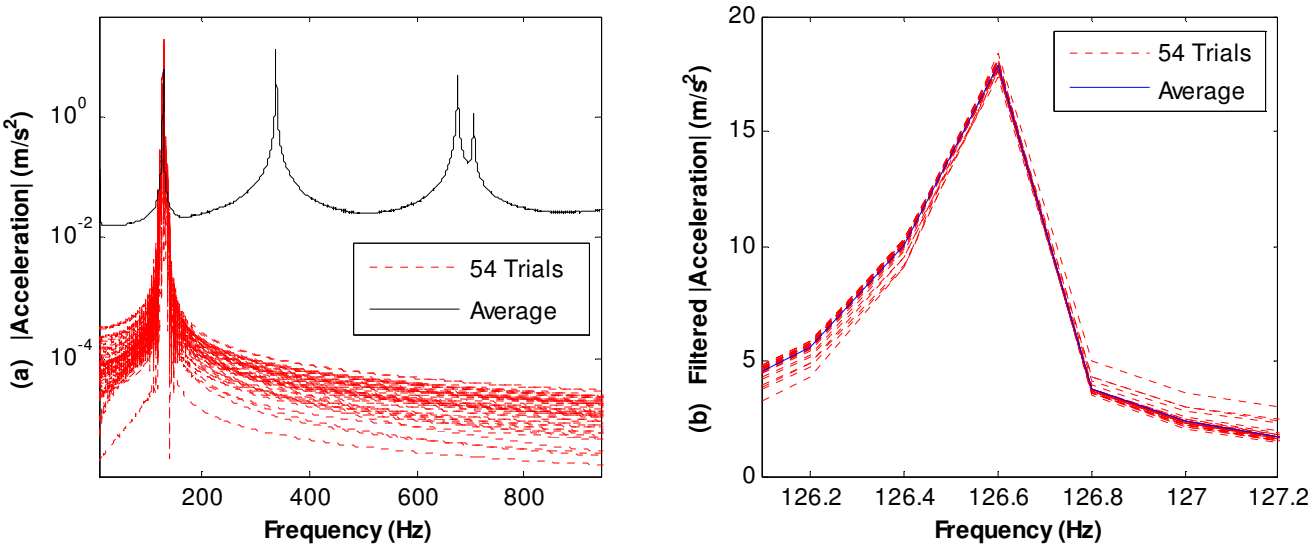

Fig. 14 (a) Filtered frequency responses of all 54 data points compared with the average of the unfiltered frequency response. (b) Filtered frequency responses after dividing by the mass normalized mode shape value; the trials are remarkably consistent.

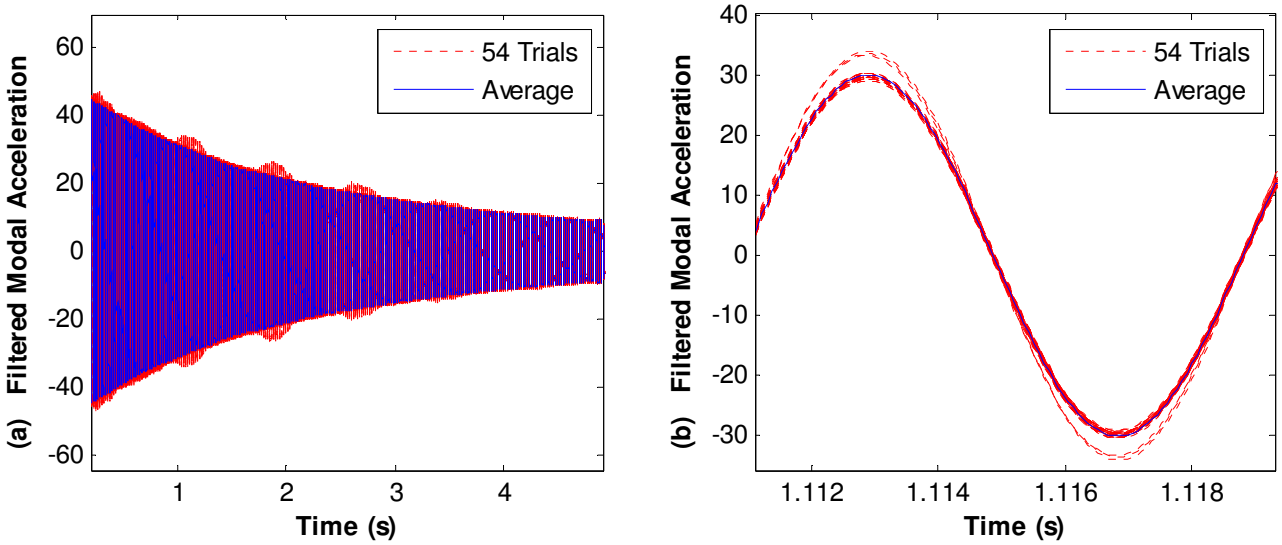

Fig. 15 (a) Modal time responses for the first mode and the averaged time response. (b) Detail view showing that the measurements were highly consistent except for three measurement points.

The responses are remarkably repeatable suggesting that the impact load provided by the automatic hammer was essentially the same from trial to trial. On the other hand, there are a few trials that differed from the others by 10% or more. For the data shown in the figures above, the amplitude of the impact force ranged from approximately 155 to 160 Newtons.

The voltage applied to the automatic hammer was adjusted so that a range of impact forces were applied to the beam. Then, the response was measured at all 54 points and this process was repeated at each impact force level.

4.5 Lab Results

Modal Iwan models were deduced from laboratory data in a similar fashion as was done in the simulation data. However, macro-slip was not clearly observed at the force levels that were used, so the parameters $\{\hat{K}_T, \hat{F}_S, \hat{\beta}\}$ were estimated and then adjusted until the modal Iwan model reproduced the measured dissipation versus force curve as well as possible. The energy dissipation per cycle for the 1st elastic mode is shown in Fig. 16.

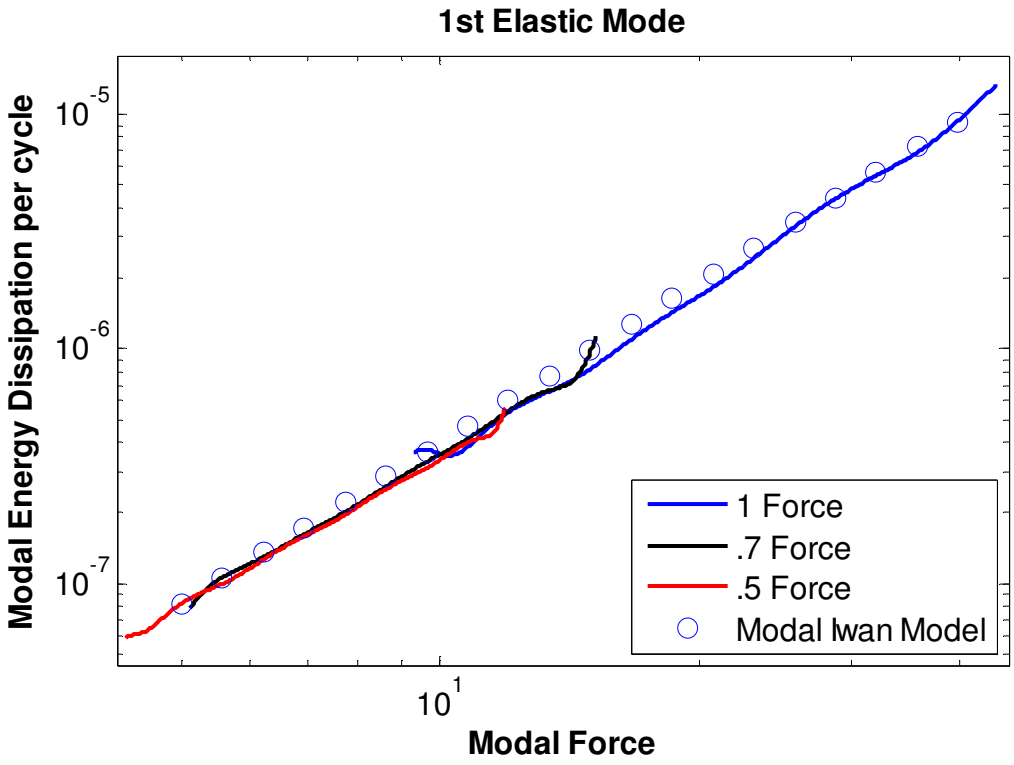

Fig. 16 Modal energy dissipation per cycle versus modal force for the 1st elastic mode.

Three different force levels were used. The notation "1 Force" indicates that the maximum voltage was given to the automatic hammer, while the 0.7 and 0.5 Force cases correspond to 70% and 50% of the maximum voltage, respectively. The measurements seem to fit the dissipation curve for the modal Iwan model quite well; however, this is a bit of an artifact of the log scale. An even better fit is obtained if each response is taken separately, but when this is done the slope of the curve changes with force level. The slope of each dissipation versus force curve is given in Table 4. At the 50% force level, the slope is 2.1 indicating a $\hat{\chi}$ value of -0.9 and a nearly linear response. The modal Iwan model used in Sec. 3.4 does not exhibit this phenomenon, but it is readily explained. Simulations of a single modal Iwan response reveal a very similar phenomenon if a linear viscous damping element is added in parallel with the Iwan joint. At low force levels the damping is dominated by the viscous damper, while at higher force levels the Iwan joint increases the dissipation and hence increases the value of $\hat{\chi}$. For this system, the viscous damping provided by the suspension system could be responsible for the linear damping seen at low force levels, although it was thought to be negligible at these force levels.

Table 4: Slope of the dissipation versus force curves for different impact force levels.

Impact Force Level	Slope	$\hat{\chi}$
1 Force	2.398	-0.602
0.7 Force	2.168	-0.832
0.5 Force	2.096	-0.904

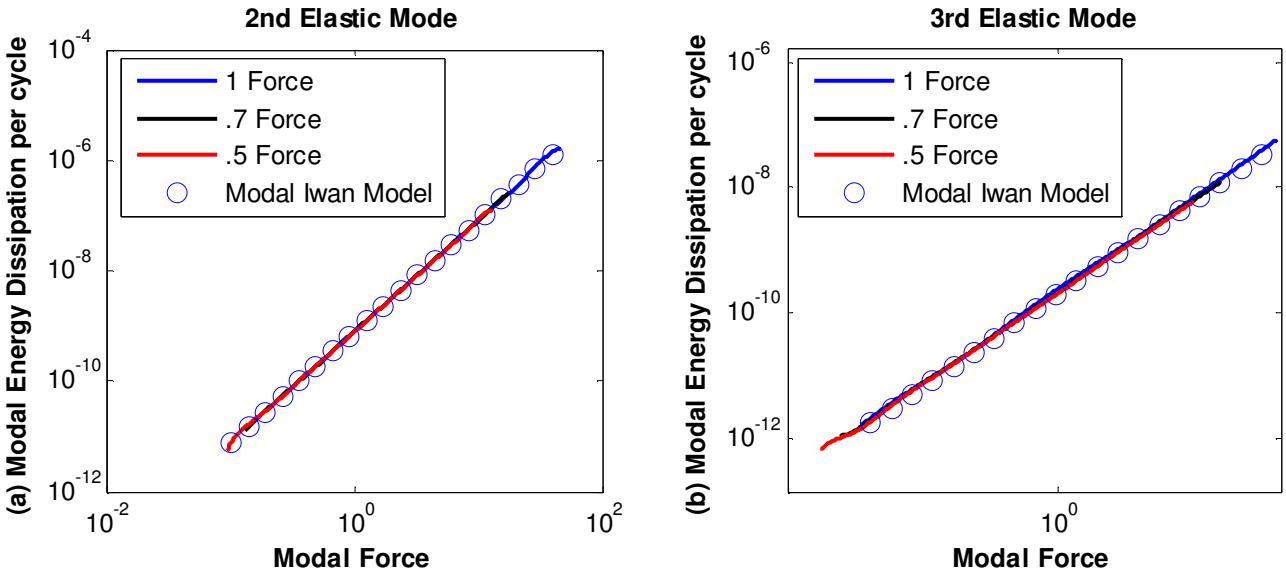

Fig. 17 Modal energy dissipation per cycle versus modal force for the 2nd (a) and 3rd (b) elastic modes.

Fig. 17 shows the modal energy dissipation versus modal force for the 2nd and 3rd elastic modes. Again, the modal Iwan model seems to fit the data quite well, on a log scale at least. The vertical axis also reveals that the energy dissipation per cycle associated with each mode seems to decrease with an increase in mode number. The dissipation curve for the 2nd elastic mode has a slope of 2.01 corresponding to a $\hat{\chi}$ value of -0.99 which is characteristic of a linear system. The $\hat{\chi}$ value for the 3rd elastic mode is -0.97, also suggesting that this mode behaves linearly. Thus, the dissipation in these modes could be modeled with a linear mode and a linear modal damping ratio instead of a modal Iwan model.

The fact that the 3rd mode exhibits linear damping is quite different from what was observed in the simulations in Sec. 3.4. There the damping in the 3rd mode seemed to be more highly nonlinear than that of the 1st mode. Note however, that in the simulation the third elastic mode did reach macro-slip at a force that was about an order of magnitude higher than what was required for the first mode, so perhaps the force levels used were insufficient to excite nonlinearity in the third mode.

5. Conclusion

This work applied the modal Iwan model developed by Segalman [5] to simulation data from a finite element model with several discrete Iwan joints and to laboratory data. The 4-parameter Iwan model was used to model the nonlinear damping associated with each mode. This model was found to fit the simulation data very well in the micro-slip region, and it agreed qualitatively well into macro-slip. This finding is encouraging; the time response of the modal Iwan model can be found in a tiny fraction of the time required to find the response of the full system with discrete Iwan joints. Further work is needed to determine whether this approach could be extended beyond macro-slip, but the results to date are fairly encouraging. Our experience revealed that while the $\hat{\chi}$ value and the joint stiffness $\hat{K}_T$ could be readily determined, the slip force $\hat{F}_S$ and $\hat{\beta}$ value were more ambiguous even when the dissipation curve was available over a wide range of forces. This suggests that it may not be advisable to extrapolate the behavior of the system to very high force levels.

On the other hand, the experimental study presented several challenges. In order to maintain similarity with the finite element simulations, a beam with a single link was tested. However, the link is small relative to the beam and seems to affect its dynamics very little. As a result, the damping effects of the joints were difficult to observe. However, the damping nonlinearity that was observable did fit the modal Iwan framework very well. This could prove highly advantageous, as the modal Iwan framework allows one to condense a very large quantity of measured data into a few physically meaningful parameters.

Acknowledgements

This work was conducted at Sandia National Laboratories. Sandia is a multi-program laboratory operated under Sandia Corporation, a Lockheed Martin Company, for the United States Department of Energy under Contract DE-AC04-94-AL85000. The authors would especially like to thank Michael Guthrie for a helpful discussion regarding the simulation

work. They are also indebted to Jill Blecke, Hartono Sumali, Randall Mayes, Brandon Zwink and Patrick Hunter for the help that they provided with the laboratory setup and testing.

References

[1] D. J. Segalman, "An Initial Overview of Iwan Modelling for Mechanical Joints," Sandia National Laboritories, Albuquerque, New Mexico SAND2001-0811, 2001.

[2] D. J. Segalman, "A Four-Parameter Iwan Model for Lap-Type Joints," *Journal of Applied Mechanics,* vol. 72, pp. 752-760, September 2005.

[3] M. S. Allen and R. L. Mayes, "Estimating the degree of nonlinearity in transient responses with zeroed early-time fast Fourier transforms," *Mechanical Systems and Signal Processing,* vol. 24, pp. 2049-2064, 2010.

[4] D. J. Segalman and W. Holzmann, "Nonlinear Response of a Lap-Type Joint using a Whole-Interface Model," presented at the 23rd International Modal Analysis Conference (IMAC-XXIII), Orlando, Florida, 2005.

[5] D. J. Segalman, "A Modal Approach to Modeling Spatially Distributed Vibration Energy Dissipation," Sandia National Laboratories, Albuquerque, New Mexico and Livermore, California SAND2010-4763, 2010.

[6] D. J. Segalman and M. J. Starr, "IWAN MODELS AND THEIR PROVENANCE," presented at the ASME 2012 International Design Engineering Technical Conference, Chicago, IL, USA, 2012.

[7] D. D. Quinn and D. J. Segalman, "Using Series-Series Iwan-Type Models for Understanding Joint Dynamics," *Journal of Applied Mechanics,* vol. 72, pp. 666-673, 2005.

[8] D. J. Segalman and M. J. Starr, "Relationship Among Certain Joints Constitutive Models," Sandia National Laboritories, Albuquerque, New Mexico SAND2004-4321, 2004.

[9] Y. Song, D. M. McFarland, L. Bergman, and A. F. Vakakis, "Effect of Pressure Distribution on Energy Dissipation in a Mechanical Lap Joint," *AIAA Journal,* vol. 43, pp. 420-425, 2005.

[10] D. O. Smallwood, D. L. Gregory, and R. G. Coleman, "Damping Investigations of a Simplified Frictional Shear Joint," Sandia National Laboratories, Albuquerque, New Mexico SAND2000-1929C, 2000.

[11] G. M. Reese, M. K. Bhardwaj, D. J. Segalman, K. Alvin, and B. Driessen, "Salinas - User's Notes," Sandia National Laboritories, Albuquerque, New Mexico SAND99-2801, 1999.

[12] G. M. Reese, T. F. Walsh, and M. K. Bhardwaj, "Salinas - Theory Manual," Sandia National Laboratories, Albuquerque, New Mexico SAND2011-8272, 2011.

[13] H. Sumali and R. A. Kellogg, "Calculating Damping from Ring-Down Using Hilbert Transform and Curve Fitting," presented at the 4th International Operational Modal Analysis Conference (IOMAC), Istanbul, Turkey, 2011.

[14] M. W. Sracic, M. S. Allen, and H. Sumali, "Identifying the modal properties of nonlinear structures using measured free response time histories from a scanning laser Doppler vibrometer," presented at the International Modal Analysis Conference XXX, Jacksonville, Florida USA, 2012.

[15] M. Feldman, "NON-LINEAR SYSTEM VIBRATION ANALYSIS USING HILBERT TRANSFORM - I. FREE VIBRATION ANALYSIS METHOD 'FREEVIB'," *Mechanical Systems and Signal Processing,* vol. 8, pp. 119-127, 1993.

[16] Q. Zhang, Allemang, R. J. , Brown, D. L., "Modal Filter: Concept and Application," presented at the 8th International Modal Analysis Conference (IMAC VIII), Kissimmee, Flordia, 1990.

[17] H. Sumali, "An experiment setup for studying the effect of bolt torque on damping," presented at the 4th International Conference on Experimental Vibration Analysis for Civil Engineering Structures (EVACES), Varenna, Italy, 2011.

[18] T. G. Carne, D. T. Griffith, and M. E. Casias, "Support Conditions for Experimental Modal Analysis," *Sound and Vibration,* vol. 41, pp. 10-16, 2007.

[19] M. S. Allen and J. H. Ginsberg, "A Global, Single-Input-Multi-Output (SIMO) Implementation of The Algorithm of Mode Isolation and Applications to Analytical and Experimental Data," *Mechanical Systems and Signal Processing,* vol. 20, pp. 1090-1111, 2006.